Dynamical Pattern Selection of Growing Cellular Mosaic in Fish Retina

Noriaki Ogawa,[1,3,*] Tetsuo Hatsuda,[1,3,†] Atsushi Mochizuki,[2,3,4,‡] and Masashi Tachikawa[2,3,§]

[1] *Theoretical Research Division, RIKEN Nishina Center, Saitama 351-0198, Japan*
[2] *Theoretical Biology Laboratory, RIKEN, Saitama 351-0198, Japan*
[3] *Interdisciplinary Theoretical Science Research Group (iTHES), RIKEN, Saitama 351-0198, Japan*
[4] *CREST, JST, Kawaguchi 332-0012, Japan*

A Markovian lattice model for photoreceptor cells is introduced to describe the growth of mosaic patterns on fish retina. The radial stripe pattern observed in wild-type zebrafish is shown to be selected naturally during the retina growth, against the geometrically equivalent, circular stripe pattern. The mechanism of such dynamical pattern selection is clarified on the basis of both numerical simulations and theoretical analyses, finding that successive emergence of local defects plays a critical role to realize the wild-type pattern. Physical and biological implications are also discussed.

PACS numbers: 87.18.Hf, 87.17.Pq, 75.10.Hk

arXiv:1610.03596v1 [q-bio.CB] 12 Oct 2016

Introduction: Arrangement of the color detecting photoreceptors (cone cells) on a retina is believed to be functionally important for animals to determine the spatial resolution of the color imaging [1]. In some teleost fishes, the cone cells sensitive to green (G ●), red (R ●), blue (B ●) and ultra-violet (UV ●) lights with G and R forming a pair called the "double cones" (GR ◐), form two-dimensional patterns: They are called the "cone mosaics" and have been known since 19th century (see e.g. [2] and references therein). However, the mechanism for the pattern formation is still unclear.

Among others, the cone mosaic of the zebrafish shown in FIG. 1 has a prominent feature with two major characteristics; directionality and long periodicity [4]. Stripes of cells run radially from the central to the marginal region of the retina, and the periodicity of the pattern differs between radial and circular directions as shown in FIG. 1(a). Although the two patterns, (a) and its $+90^\circ$ rotation (b), have the same c2mm symmetry of the wallpaper group [3] and have thus the same binding energy, only the pattern (a) is realized in nature. In this paper, we refer (a) as the "radial" ($*$) stripe pattern since it is along with the growing direction of the retina, and (b) as the "circular" ($\odot$) one.

In adult fish, a retina continuously grows through its life by generating new photoreceptors in the germinal zone of retinal margin called the ciliary marginal zone (CMZ). The rearrangement of those new cone cells *after* cellular differentiation is considered to play a crucial role for mosaic pattern formation. This is supported by a cell-trace experiment in which most of the cells are found not to change their subtypes after the first determination [5].

Theoretically, cell rearrangement models for cone mosaics have been formulated on a two-dimensional square lattice: It was found that different patters (such as the zebrafish pattern with c2mm symmetry and the medaka pattern with p4mg symmetry) can be generated successfully by stochastic cell movements biased by appropriate cell-cell adhesion force [6–8]. However, such models have failed to distinguish the characteristics of directionality,

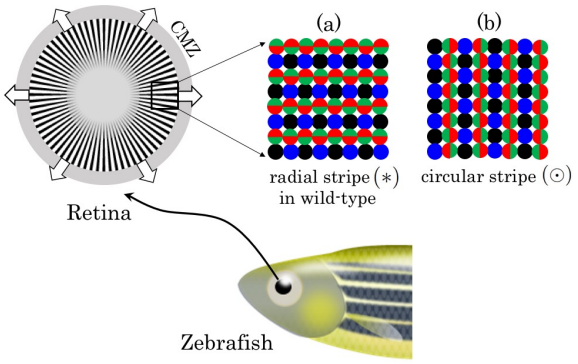

FIG. 1: Schematic picture of the Zebrafish retina and possible cone mosaic patterns. Typical size of the retina and the cone cell are several hundred μm (3-4 days after fertilization) and a few μm (along with the retina surface), respectively. The ciliary marginal zone (CMZ) where new cone cells are bone is denoted by gray area surrounding the retina.

such as the distinction between (a) and (b) in FIG. 1. The main purpose of this paper is to propose a new mechanism in which the sequential accretion of new cone cells from CMZ triggers dynamical pattern selection (DPS) among those with the same binding energy. We demonstrate it explicitly by taking the zebrafish as a characteristic example.

Markovian Lattice Model for Pattern Formation: To take into account the fact that retina grows dynamically by receiving new cone cells born in CMZ, we extract a rectangular region of the retina margin as indicated in FIG. 1 and introduce a Markovian model where cone cells are supplied stochastically from the "CMZ pool" to the two-dimensional lattice of cells column-by-column as shown in FIG. 2(a). The radial growth of the actual retina is represented by the horizontal growth toward the right direction. The vertical size of the lattice is denoted by w. Possible formation of dislocations in the realistic radial growth will not be considered in this paper. The growth is dictated by the action of a transition matrix

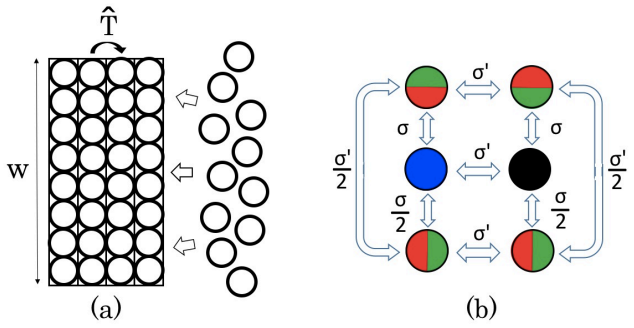

FIG. 2: (a) Radial growth of a part of the fish retina with a vertical size w due to the accretion of new cone cells. The transition matrix from one column to the next is denoted by $\hat{T}$. (b) Binding energies between neighboring sites for Zebrafish patterns.

$\hat{T}$ whose explicit form will be specified shortly. In the CMZ pool, we consider B, UV and the double cone (RG) with the number ratio, 1:1:2, anticipating the possible stripe structures in FIG. 1(a,b). Then, we have six degrees of freedom on each lattice site with the probability, ● : ● : ◑ : ◒ : ◑ : ◒ $= \frac{1}{4} : \frac{1}{4} : \frac{1}{8} : \frac{1}{8} : \frac{1}{8} : \frac{1}{8}$.

The binding energies between the neighboring cells, σ_{pq} with p and q taking either B, R, G, or UV, would be dictated by the binding proteins on the cone cell membranes, although the specific protein structures are not yet fully identified experimentally. Previous analyses of the "phase diagram" of cell patterns in the multi-dimensional σ_{pq}-space in the stochastic rearrangement models [6, 7] show that the zebrafish patterns, FIG. 1(a,b), are equally realized as stationary states if the three inequalities below are simultaneously satisfied [12]: $3\sigma_{\rm RG} - \sigma_{\rm BU} < \sigma_{\rm BR} + \sigma_{\rm UG}, 3\sigma_{\rm BU} - \sigma_{\rm RG} < \sigma_{\rm BR} + \sigma_{\rm UG}, \sigma_{\rm BR} + \sigma_{\rm UG} < 2(\sigma_{\rm BU} + \sigma_{\rm RG}) - (\sigma_{\rm BG} + \sigma_{\rm UR})$. We take these inequalities as guide lines to choose cell bindings: our particular choice of σ_{pq} is shown in FIG. 2(b):

$$\sigma \equiv \sigma_{\rm BR} = \sigma_{\rm UG}, \quad \sigma' \equiv \sigma_{\rm BU} = \sigma_{\rm RG} \quad (1 < \sigma/\sigma' < 2),$$
$$\sigma_{\rm BG,UR,BB,RR,GG,UU} = 0. \tag{1}$$

The binding energies to the double cones are assumed to be proportional to the contact area, e.g. the side-by-side coupling between ● and ◒ is chosen to be $(\sigma_{\rm BG} + \sigma_{\rm BR})/2$. Therefore, in FIG. 2(b), we have $\sigma'/2 < \sigma/2 < \sigma' < \sigma$. In our analyses below, we take a specific value $\sigma/\sigma' = 3/2$: We have checked that essential conclusions of our paper are unchanged as long as $1 < \sigma/\sigma' < 2$.

In the Markov chain shown in FIG. 2(a), the lattice sites are empty at the beginning and the six types of cone cells in FIG. 2(b) occupy the sites column-by-column in a stochastic manner. Each column with periodic boundary condition in the vertical direction has 6^w different configurations labeled by the index $j(= 1, 2, \cdots, N = 6^w)$. The probability of having the configuration j in the n-th column is defined as $P_j^{(n)}$ so that the probability vector for the n-th column reads $\mathbb{P}^{(n)} \equiv (P_1^{(n)}, P_2^{(n)}, \cdots, P_N^{(n)})^{\rm T}$ with $\sum_j P_j^{(n)} = 1$, where $(\cdots)^{\rm T}$ denotes the transpose ($-90°$ rotation). The Markov chain is generated by the $N \times N$ transition matrix $\hat{T}$ as

$$\mathbb{P}^{(n+1)} = \hat{T}\mathbb{P}^{(n)}, \tag{2}$$

where the matrix element T_{ij} with $\sum_{i=1}^N T_{ij} = 1$ is nothing but the probability of having a configuration i in the $(n+1)$-th column given the configuration j in the n-th column.

To model the retinal growth, we consider T_{ij} having a Boltzmann form with an "effective" temperature β^{-1}:

$$T_{ij} = \frac{p_i e^{-\beta \mathcal{E}_{ij}}}{N_j}, \quad N_j = \sum_i p_i e^{-\beta \mathcal{E}_{ij}},$$
$$\mathcal{E}_{ij}(\sigma, \sigma') = -B_i^{(\rm intra)} - B_{ij}^{(\rm inter)} \le 0. \tag{3}$$

Here $B_i^{(\rm intra)}$ is a sum of the intra binding energies in the configuration i, while $B_{ij}^{(\rm inter)}$ is a sum of the inter binding energies between i and j. The prior probability factor p_i is computed by taking into account the number ratio of the cone cells in the CMZ pool: For example, $p_i = \frac{1}{4} \times \frac{1}{8} \times \frac{1}{4} \times \frac{1}{8}$ for $i = (●◑◒◑◒)^{\rm T}$. Physically, β^{-1} corresponds to the mobility of the cone cells and introduces fluctuations to the cell pattern formation. Since $\mathcal{E}_{ij}$ is a linear function of σ and σ', $\beta\mathcal{E}_{ij}$ and T_{ij} can be written in terms of the dimensionless variables, $t \equiv 2/\beta\sigma'$ (reduced temperature) and σ/σ' (coupling ratio). By definition, the fluctuation becomes large as t increases.

For later convenience, we introduce a bra-ket notation: Each configuration i is represented by a state vector $|i\rangle$, so that $T_{ij} = \langle i|\hat{T}|j\rangle$. The eigenvalues of $\hat{T}$ and the corresponding left-right eigenvectors are defined by $\langle l|\hat{T} = \langle l|\lambda_l$ and $\hat{T}|l\rangle = \lambda_l|l\rangle$ $(l = 1, 2, \cdots, N)$ with a relative normalization, $\langle l|l'\rangle = \delta_{ll'}$. Then, we have

$$\hat{T}^n = \sum_l |l\rangle\lambda_l^n\langle l|, \quad \mathbb{P}^{(n)} = \sum_l c_l\lambda_l^n|l\rangle, \tag{4}$$

where c_l's are the expansion coefficients at $n = 0$. Note that λ_l's are in general complex, since $\hat{T}$ is non-symmetric.

At $t = 0$, $\hat{T}$ is reducible, i.e., there appears multiple closed subspaces and $\mathbb{P}^{(\infty)}$ is not unique. Correspondingly, there arises multiple eigenvectors with the eigenvalue 1. For $t > 0$, all the components of $\hat{T}$ is positive, so that finite Markov chain becomes irreducible and aperiodic [9]. Consequently, there exists a unique probability vector $\mathbb{P}^{(\infty)}$ irrespective of the initial vector. Moreover, the Perron-Frobenius theorem for positive matrix implies that (i) there is only one left eigenvector $\langle l = 1| = (1, 1, 1, \cdots)$ with $\lambda_{l=1} = 1$, and (ii) the absolute values of other eigenvalues obey $|\lambda_l| < 1$, with the sum of components for each right eigenvectors being 0 due to $\langle l = 1|l' \ne 1\rangle = 0$. Note that the property (i) and

$\sum_j P_j^{(0)} = 1$ imply $c_1 = 1$ in Eq.(4). The essential question in DPS, after all, is to identify a particular pattern which dominates the state $|l = 1\rangle$ at $n \to \infty$.

Stationary patterns at $t = 0$: For zero effective temperature, the following 8 columns play crucial roles for pattern formation: (A) $(\bullet\bullet\bullet\bullet\cdots)^{\mathrm{T}}$, (B) $(\bullet\bullet\bullet\bullet\cdots)^{\mathrm{T}}$, (C) $(\bullet\bullet\bullet\bullet\cdots)^{\mathrm{T}}$, (D) $(\bullet\bullet\bullet\bullet\cdots)^{\mathrm{T}}$, (E) $(\bullet\bullet\bullet\bullet\cdots)^{\mathrm{T}}$, (F) $(\bullet\bullet\bullet\bullet\cdots)^{\mathrm{T}}$, (G) $(\bullet\bullet\bullet\bullet\cdots)^{\mathrm{T}}$, (H) $(\bullet\bullet\bullet\bullet\cdots)^{\mathrm{T}}$, where $\cdots$ denotes the repetition. Note that (A)-(D) have the same intra-binding energy, a multiple of σ, while (E)-(H) has the same intra-binding energy, a multiple of σ'. In terms of the bra-ket notation, $|A\rangle = (1, 0, 0, 0, \cdots)^{\mathrm{T}}$, $|B\rangle = (0, 1, 0, 0, \cdots)^{\mathrm{T}}$, $|C\rangle = (0, 0, 1, 0\cdots)^{\mathrm{T}}$, etc. Then, $\hat{T}_0$ (the transition matrix at $t = 0$) in the state-space spanned by $\mathcal{M} \equiv \{A, B, C, D, E, F, G, H\}$ and the others are reducible and sparse:

$$\hat{T}_0 = \begin{array}{c} \begin{array}{cccc} A & B & C & D \quad E \quad F \quad G \quad H \quad \cdots \end{array} \\ \left(\begin{array}{cc|c} \begin{array}{cccc} 0&1&0&0\\1&0&0&0\\0&0&0&1\\0&0&1&0\end{array} & \multirow{2}{*}{0} & \multirow{2}{*}{$\cdots$} \\ \multirow{2}{*}{0} & \begin{array}{cccc} 0&0&0&1\\1&0&0&0\\0&1&0&0\\0&0&1&0\end{array} & \\ \hline & 0 & \ddots \end{array}\right) \end{array}. \tag{5}$$

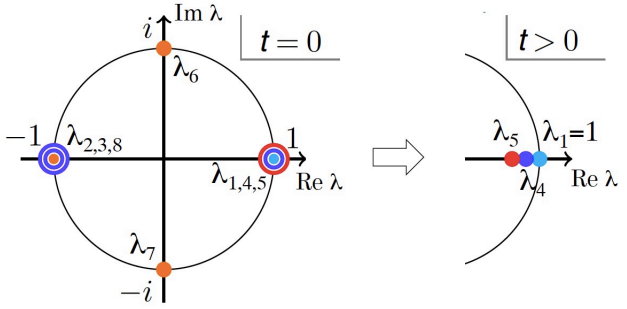

FIG. 3: Major (largest 8) eigenvalues of $\hat{T}$ at $t = 0$ (left) and those close to $\lambda = 1 + 0i$ for $t > 0$ (right). The cyan and blue points corresponds to the eigenmodes responsible for the radial stripes, while the red and orange ones are for the circular stripes. At finite t, the cyan ($l = 1$) does not move, whereas the others go toward the inner direction.

Due to the fact that $(\hat{T}_0)_{i\notin\mathcal{M}, j\in\mathcal{M}} = 0$, all the probability flows into the subspace $\mathcal{M}$, while it does not flow out from $\mathcal{M}$. Furthermore, the subspace $\mathcal{M}$ is reducible to three closed sets, $\{A, B\}$, $\{C, D\}$, and $\{E, F, G, H\}$, so that they respectively form the following stable patterns;

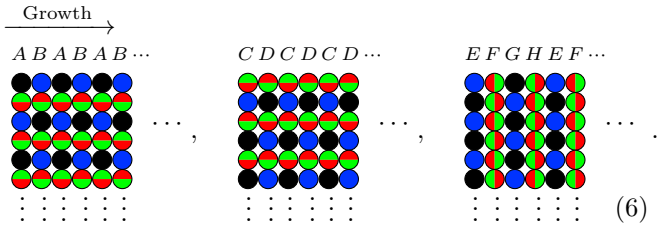

(6)

The first two patterns, which are equivalent under periodic boundary condition in circular direction, correspond to the radial stripe pattern of the wild-type zebrafish in FIG. 1(a), while the third one corresponds to the circular stripe pattern in FIG. 1(b).

Corresponding to the multi-stability due to the reducibility of (5), there arise eight eigenvectors $\{|l\rangle\}_{l=1\ldots8}$ with $|\lambda_l| = 1$. They have nonzero components only in $\mathcal{M}$. Such degeneracy is removed under infinitesimal fluctuation at finite t, due to the positivity of T_{ij}. The major eight eigenvalues for $t = 0$ and the eigenvalues near $\lambda = 1$ for small positive t are sketched in FIG. 3. The detailed analysis of these eigenvalues is given in the Supplemental Material I.

Dynamical pattern selection (DPS) at $t \neq 0$: Let us now study DPS at finite effective temperature (finite cell mobility) by performing a stochastic simulation with the transition matrix (3). At each n-th column ($n \geq 1$), we start with a random configuration and sweep through all the sites inside the column by N_{sw} times using the Metropolis update with $\mathcal{E}_{ij}$. Then we fix the configuration and go to the $(n + 1)$-th column. This procedure gives a single pattern (a trajectory) for each trial starting from an initial configuration at $n = 0$. By repeating this procedure either by changing or keeping the initial condition, trajectories with total number $N_{\mathrm{traj.}}$ are generated. One may consider each trajectory as a pattern realized in individual zebrafish. Mean properties of the patterns can be obtained by averaging over the trajectories.

Shown in the upper panels of FIG. 4 are two examples sampled from 4096 trajectories with random initial configurations at $n = 0$ with $w = 16$ (about 10% of the retina circumference) and $N_{\mathrm{sw}} = 2^{17-18}$ (large enough for thermalization). From the simulations carried out for $t = 0.2 - 0.5$, examples at $t = 0.4$ are displayed in the figure: Although the radial stripes and circular stripes are stationary patterns equally possible at $t = 0$, the dynamical retina growth at $t > 0$ selects the radial stripes observed in wild-type zebrafish irrespective of the initial random configurations.

In order to quantify similarity of a configuration at given n with the radial and circular stripes, let us introduce a *similarity measure*. First, we note that the radial stripe pattern at given n consists of the basic units $\{(\bullet\bullet)^{\mathrm{T}}, (\bullet\bullet)^{\mathrm{T}}, (\bullet\bullet)^{\mathrm{T}}, (\bullet\bullet)^{\mathrm{T}}\}$, while the circular stripe pattern consists of $\{(\bullet\bullet)^{\mathrm{T}}, (\bullet\bullet)^{\mathrm{T}}, (\bullet\bullet)^{\mathrm{T}}, (\bullet\bullet)^{\mathrm{T}}\}$. Then, we count

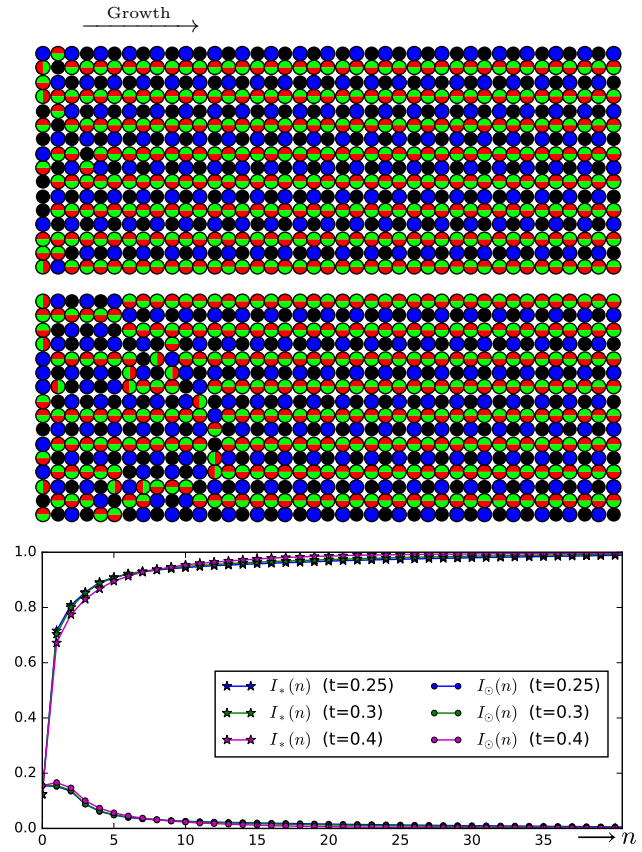

FIG. 4: Upper panels: Two cases sampled from 4096 trajectories with random initial configuration for $w = 16$ and $t = 0.4$. Lower panel: Similarity measures $I_*(n)$ (star) and $I_\odot(n)$ (circle) at $t = 0.25$, 0.3, 0.4 averaged over 4096 trajectories.

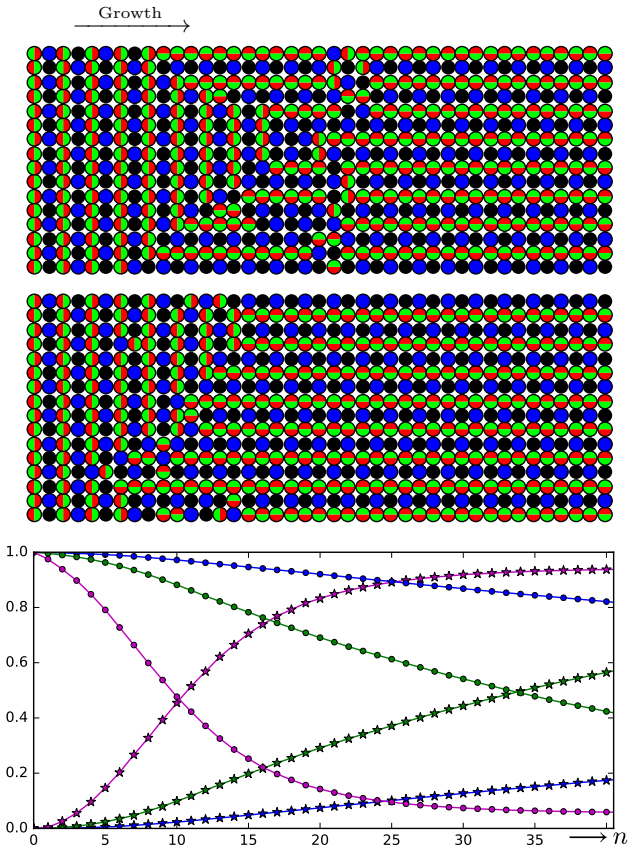

FIG. 5: Upper panels: Two cases sampled from 2048 trajectories with F-type initial configuration for $w = 16$ and $t = 0.4$. Lower panel: $I_{*,\odot}(n)$ at $t = 0.25$, 0.3, 0.4, averaged over 2048×4 trajectories under (E, F, G, H) initial configurations with equal weight. The legend is the same with FIG. 4.

how many basic units are contained in a column at given n. Dividing the resultant number by w and averaging it over trajectories, we obtain the similarity measures $I_*(n)$ and $I_\odot(n)$. They are plotted by filled stars and filled circles in the lower panels of FIG. 4 as a function of n for $t = 0.25, 0.3$ and 0.4. One finds that $I_*(n)$ ($I_\odot(n)$) approaches to 1 (0) quickly as n increases with weak t-dependence. Thus, FIG. 4 indicates that the radial stripe pattern is the true asymptotic configuration corresponding to $\mathbb{P}^{(\infty)}$.

To check whether the circular stripe pattern is indeed unstable, we consider circular-type (E, F, G, H) initial configurations in FIG. 5. The upper panels show two cases sampled from 2048 trajectories with the F-type initial configuration. Under the dynamical retina growth at $t > 0$, the circular stripe pattern turns into the radial stripe after certain steps. Close look at the figure shows that the transition from the circular stripes to the radial stripes is initiated by the creation and propagation of small local defects. Plotted in the lower panel of FIG. 5 are the similarity measures averaged over (E, F, G, H)-stripe initial configurations. In this case, approach to the radial stripe pattern becomes slower as t decreases, as expected by the formation probability of small defects.

Let us finally discuss the essential mechanism of DPS in terms of the eigenvalues and eigenvectors of $\hat{T}$. The similarity measure with $R = *, \odot$ can be written as

$$I_R(n) = \sum_{j=1}^{N} I_R^j P_j^{(n)} = \sum_{l=1}^{N} c_l I_R^{(l)} \lambda_l^n, \tag{7}$$

where I_R^j is the similarity measure of a state $|j\rangle$ to R, and $I_R^{(l)} \equiv \sum_j I_R^j \langle j|l\rangle$. For small t, $I_*^{(1,5)}$ and $I_\odot^{(5)}$ are close to 1, while others are close to 0 (Eq.(S.22) in Supplemental Material I). Therefore, for large n, we have $I_*(n) \to I_*^{(1)} + c_5 I_*^{(5)} \lambda_5^n \simeq 1$ (for $n \to \infty$) and $I_\odot(n) \to c_5 I_\odot^{(5)} \lambda_5^n \simeq 0$ (for $n \to \infty$). Here $\lambda_5 = 1 - \mathcal{O}(g^2)$ corresponds to the eigenvector $|5\rangle \propto (-1, -1, -1, -1, 1, 1, 1, 1, \vec{0})^{\mathrm{T}} + \mathcal{O}(g^2)$ which swaps the radial and circular stripe patterns. These are consistent with what are shown in FIG. 4 and FIG. 5. One may also extract the transition step scale by fitting the data in these figures, $I_\odot(n) \sim \lambda_5^n = \exp(-n/\bar{n})$ with

$\bar{n}^{-1} = -\ln\lambda_5 \simeq (11.6 \pm 1.4)g^2$ and $g = e^{-1/t}$ (see Eq.(S.30) in Supplemental Material II). Thus, the mean number of steps for the circular stripes to decay is found to be $\bar{n} = 13.0 \pm 1.6$ for $t = 0.4$.

The escape rates from the radial and circular patterns are critical for DPS. They are governed by the smallest deficit energies from the patterns (Supplemental Material III),

$$\Delta\mathcal{E}_* = \min_{X\neq B}\{\mathcal{E}_{XA}\} - \mathcal{E}_{BA}, \tag{8}$$

$$\Delta\mathcal{E}_\odot = \min\left\{\min_{X\neq F}\{\mathcal{E}_{XE}\} - \mathcal{E}_{FE}, \min_{X\neq G}\{\mathcal{E}_{XF}\} - \mathcal{E}_{GF}\right\}.$$

The configuration having larger $\Delta\mathcal{E}$ survives at large n. Under the choice in (1), we have

$$\Delta\mathcal{E}_* = \sigma > \sigma' = \Delta\mathcal{E}_\odot, \tag{9}$$

which confirms the survival of the radial stripes [13].

Summary and discussion In this Letter, we have introduced a Markovian lattice model to describe the dynamics of cone-cell mosaic patterns in growing retina. With numerical simulations in the 6^w-dimensional state-space ($w = 16$) together with theoretical analyses of eigenvalues and eigenvectors of the transition matrix $\hat{T}$, we found that the growing process naturally selects the radial stripe pattern observed in the wild-type zebrafish against the circular stripe pattern. Such a "dynamical pattern selection (DPS)" could not be described by the previous no-growth models. Successive appearance of small defects during the growth plays a key role to transfer arbitrary patterns to the radial stripes.

In the present study, we chose the cell-cell bindings σ_{pq} to be characteristic values for the zebrafish, while the effective temperature t corresponding to cell mobility was treated as a free parameter. To make further connection of t and σ_{pq} to microscopic cell dynamics, it would be necessary to make quantitative comparison of our model predictions to in vivo experimental data for the growth rate of the pattern and also for the defect frequencies with wild-type and mutant embryos. Also, numerical simulations with round shaped retina needs to be carried out for realistic comparison with data. Direct measurements of cell-cell bindings using the atomic force microscope [10] would also give useful information on σ_{pq}.

Although we have focused on cellular mosaic patterns in this Letter, they have suggestive similarities with other examples in non-equilibrium physics, such as the crystal growth, patterns in granular materials, copolymerization etc, where various spatial or temporal patterns emerge due to infinitesimally small perturbations [11]. Our theoretical approach may provide a novel insight into a universal description of DPS in life and matter.

The authors thank Sachihiro C. Suzuki, Ichiro Masai, Yuko Nishiwaki and Bernold Fiedler for valuable discussions and comments. This work was supported by RIKEN iTHES Project.

* Electronic address: noriaki@riken.jp
† Electronic address: thatsuda@riken.jp
‡ Electronic address: mochi@riken.jp
§ Electronic address: mtach@riken.jp

[1] See e.g., J. E. Cook, in *The Visual Neurosciences*, eds. L.M. Chalupa and J.S. Werner (MIT Press, Cambridge MA, 2003). S. J. Eglen, Math. Med. Biol. **23**, 79-99 (2006).
[2] A. H. Lyall, Quarterly Journal of Microscopical Science, **3.41**, 101-110 (1957); *ibid.*, **3.42**, 189-201 (1957). K. Engström, Acta Zoologica, **44**, 179-243 (1963).
[3] D. Schattschneider, American Math. Monthly. **85**, 439-450 (1978).
[4] J. M. Fadool and J. E. Dowling, Prog. in Retinal and Eye Research, **27**, 89 (1999).
[5] S. C. Suzuki *et al.*, PNAS **110**, 15109 (2013).
[6] S. Tohya, A. Mochizuki and Y. Iwasa, J. of Theor. Biol., **200**, 231 (1999).
[7] A. Mochizuki, J. of Theor. Biol., **215**, 345 (2002).
[8] S. Tohya, A. Mochizuki and Y. Iwasa, J. of Theor. Biol., **221**, 289 (2003).
[9] O. Häggström, *Finite Markov Chains and Algorithmic Applications*, (Cambridge Univ. Press, 2002).
[10] M. Krieg, Y. Arboleda-Estudillo, P.-H. Puech, J. Käfer, F. Graner, D. J. Müller and C.-P. Heisenberg, Nature Cell Biology **10**, 429 (2008).
[11] J. P. Gollub and J. S. Langer, Rev. Mod. Phys. **71**, S396 (1999).
[12] For other cases such as the Medaka pattern, σ_{pq} with p, q taken not only for neighboring cells but also for the diagonal cells is known to be necessary [8].
[13] To derive (9), we considered only *local* defects for X in (8). For σ/σ' being close to 2, *global* defects may also contribute. This indicates the emergence of a new pattern other than the radial or circular stripes. It is an interesting problem to be studied, but is beyond the scope of the present paper.

Supplemental Material

I. Perturbation theory for the transition matrix

Here we show a perturbation analysis of the transition matrix at low temperature t in terms of the expansion parameter,

$$g \equiv e^{-1/t}. \tag{S.1}$$

We consider the $6^w \times 6^w$ transition matrix where w is a multiples of 4, i.e., $w = 4w_0$ with $w_0 = 2, 3, 4, \cdots$. The numerical results shown in the text correspond to $w = 4w_0 = 16$. The transition matrix at low t can be expanded by g around $\hat{T}_0$ in Eq.(5). For Eq.(1) with $\sigma/\sigma' = 3/2$, we have

$$\hat{T} = \hat{T}_0 + \sum_{\alpha=\frac{1}{2},1,\frac{3}{2},\frac{5}{2}} g^\alpha \hat{T}_\alpha + g^2 \hat{T}_2 + g^3 \hat{T}_3 + \mathcal{O}(g^{7/2}), \tag{S.2a}$$

with

$$\hat{T}_0 = \left(\begin{array}{c|c|c} \begin{smallmatrix} 0&1&0&0\\1&0&0&0\\0&0&0&1\\0&0&1&0 \end{smallmatrix} & 0 & P_0 \\ \hline 0 & \begin{smallmatrix} 0&0&0&1\\1&0&0&0\\0&1&0&0\\0&0&1&0 \end{smallmatrix} & \\ \hline 0 & & Q_0 \end{array}\right), \qquad \hat{T}_\alpha = \left(\begin{array}{c|c|c} 0 & 0 & P_\alpha \\ \hline 0 & 0 & \\ \hline 0 & & Q_\alpha \end{array}\right) \qquad \left(\alpha = \frac{1}{2}, 1, \frac{3}{2}, \frac{5}{2}\right),$$

$$\hat{T}_2 = \left(\begin{array}{c|cccc|c} 0 & \multicolumn{4}{c|}{0} & \\ \hline 0 & 0 & 0 & 0 & -\mu_2 w_0 & \\ & -\mu_1 w_0 & 0 & 0 & 0 & \cdots \\ & 0 & -\mu_2 w_0 & 0 & 0 & \\ & 0 & 0 & -\mu_1 w_0 & 0 & \\ \hline 0 & \multicolumn{4}{c|}{J} & \ddots \end{array}\right),$$

$$\hat{T}_3 = \left(\begin{array}{cccc|cccc|c} 0 & -\nu w_0 & 0 & 0 & \multicolumn{4}{c|}{0} & \\ -\nu w_0 & 0 & 0 & 0 & & & & & \\ 0 & 0 & 0 & -\nu w_0 & & & & & \\ 0 & 0 & -\nu w_0 & 0 & & & & & \\ \hline \multicolumn{4}{c|}{0} & 0 & 0 & 0 & -\xi_2 w_0 & \\ & & & & -\xi_1 w_0 & 0 & 0 & 0 & \cdots \\ & & & & 0 & -\xi_2 w_0 & 0 & 0 & \\ & & & & 0 & 0 & -\xi_1 w_0 & 0 & \\ \hline K & & L & & \multicolumn{4}{c|}{M} & \ddots \end{array}\right), \tag{S.2b}$$

where P_0, P_α, Q_0, Q_α, J, K, L and M are the matrices with the sizes, $8\times(6^w-8)$, $8\times(6^w-8)$, $(6^w-8)\times(6^w-8)$, $(6^w-8)\times(6^w-8)$, $(6^w-8)\times 4$, $(6^w-8)\times 2$, $(6^w-8)\times 2$ and $(6^w-8)\times 4$, respectively. With the probability discussed in the main text, $\bullet:\bullet:\bullet:\bullet:\bullet:\bullet=\frac{1}{4}:\frac{1}{4}:\frac{1}{8}:\frac{1}{8}:\frac{1}{8}:\frac{1}{8}$, the numerical factors in the above matrices are computed explicitly as

$$\mu_1=8,\quad \mu_2=3,\quad \nu=5,\quad \xi_1=32,\quad \xi_2=6. \tag{S.3}$$

For later convenience, we define

$$\hat{S}\equiv\hat{T}_0+\sum_{\alpha=\frac{1}{2},1,\frac{3}{2},\frac{5}{2}} g^\alpha\hat{T}_\alpha,\quad P\equiv P_0+\sum_{\alpha=\frac{1}{2},1,\frac{3}{2},\frac{5}{2}} g^\alpha P_\alpha,\quad Q\equiv Q_0+\sum_{\alpha=\frac{1}{2},1,\frac{3}{2},\frac{5}{2}} g^\alpha Q_\alpha, \tag{S.4}$$

Note that both $\hat{T}_0$ and $\hat{S}$ are reducible and non-symmetric matrices. Also they have the same 8×8 matrix in the upper left corner. Because of these properties, they share 8 eigenvalues with $|\lambda^{(0)}_{l=1,\cdots,8}|=1$. We label these eigenvalues and corresponding left (right) eigenvectors of $\hat{S}$ as

$$\lambda^{(0)}_l,\quad \langle l^{(0)}|=\Big(\vec{x}_l,\ \vec{r}_l\Big),\quad |l^{(0)}\rangle=\Big(\vec{y}_l,\ \vec{0}\Big)^{\mathrm{T}},\quad (l=1,\cdots,8), \tag{S.5}$$

with

$$\lambda^{(0)}_1=1,\qquad \vec{x}_1=(1,1,1,1,1,1,1,1),\qquad \vec{y}_1=\frac{1}{4}(1,1,1,1,0,0,0,0), \tag{S.6a}$$
$$\lambda^{(0)}_2=-1,\qquad \vec{x}_2=(1,-1,0,0,0,0,0,0),\qquad \vec{y}_2=\frac{1}{2}(1,-1,0,0,0,0,0,0), \tag{S.6b}$$
$$\lambda^{(0)}_3=-1,\qquad \vec{x}_3=(0,0,1,-1,0,0,0,0),\qquad \vec{y}_3=\frac{1}{2}(0,0,1,-1,0,0,0,0), \tag{S.6c}$$
$$\lambda^{(0)}_4=1,\qquad \vec{x}_4=(1,1,-1,-1,0,0,0,0),\qquad \vec{y}_4=\frac{1}{4}(1,1,-1,-1,0,0,0,0), \tag{S.6d}$$
$$\lambda^{(0)}_5=1,\qquad \vec{x}_5=(0,0,0,0,1,1,1,1),\qquad \vec{y}_5=\frac{1}{4}(-1,-1,-1,-1,1,1,1,1), \tag{S.6e}$$
$$\lambda^{(0)}_6=i,\qquad \vec{x}_6=(0,0,0,0,1,i,-1,-i),\qquad \vec{y}_6=\frac{1}{4}(0,0,0,0,1,-i,-1,i), \tag{S.6f}$$
$$\lambda^{(0)}_7=-i,\qquad \vec{x}_7=(0,0,0,0,1,-i,-1,i),\qquad \vec{y}_7=\frac{1}{4}(0,0,0,0,1,i,-1,-i), \tag{S.6g}$$
$$\lambda^{(0)}_8=-1,\qquad \vec{x}_8=(0,0,0,0,1,-1,1,-1),\qquad \vec{y}_8=\frac{1}{4}(0,0,0,0,1,-1,1,-1), \tag{S.6h}$$

and the residual vectors,

$$\vec{r}_l=\vec{x}_l P\big(\lambda^{(0)}_l-Q\big)^{-1}. \tag{S.7}$$

Here the left and right eigenvectors satisfy $\langle l^{(0)}|l'^{(0)}\rangle=\delta_{ll'}$. We have chosen particular bases within the same eigenvalue as shown above for later convenience. Since the sum of each columns of Q is equal to or smaller than 1, the absolute magnitude of each eigenvalue of Q is smaller than 1, so that $\big(\lambda^{(0)}_l-Q\big)^{-1}$ in (S.7) always exists. Also, we have $\vec{r}_1=(1,1,1,\dots)\equiv\vec{1}$.

Now, we consider the effects of the first-order perturbation given by $\hat{T}_{2,3}$ in (S.2). Since the eigenvalues $+1$ and -1 have triple degeneracy, respectively, we need to diagonalize $\hat{T}_{2,3}$ in each degenerate subspace according to the degenerate perturbation theory. Then we obtain the general form of the eigenvalues,

$$\lambda=\lambda^{(0)}+ag^2+bg^3+\mathcal{O}(g^4). \tag{S.8}$$

Here a and b are written in terms of the matrix elements of P,Q,J,K,L,M. Note that the coefficients a and b depend on g, since P and Q are the function of g. In case that we need to obtain a strict power series expansion of λ in terms of g, further expansions of $a(g)$ and $b(g)$ should be made.

Perturbation in $\lambda^{(0)}_{1,4,5}=1$ subspace

The eigenspace with $\lambda^{(0)}=1$ in the unperturbed system is spanned by the $l=1,4,5$ eigenvectors. Then, $\hat{T}_2$ is expressed by a 3×3 matrix as

$$\langle l^{(0)}|\hat{T}_2|l'^{(0)}\rangle_{(l,l')\in\{1,4,5\}^2}=\begin{pmatrix}0&0&0\\0&0&0\\0&0&\frac{1}{4}\vec{r}_5\cdot\vec{j}-\frac{1}{2}(\mu_1+\mu_2)w_0\end{pmatrix}\quad\text{with}\quad\vec{j}\equiv J\begin{pmatrix}1\\1\\1\\1\end{pmatrix}. \tag{S.9}$$

where we used $\vec{r}_4\cdot\vec{j}=0$ obtained from the symmetry of 1-cell shift. (Due to the periodic boundary condition, our model is invariant under the 1-cell shift of each column, e.g. $(\bullet\bullet\bullet\bullet\bullet\bullet\bullet\bullet)^{\mathrm{T}}\to(\bullet\bullet\bullet\bullet\bullet\bullet\bullet\bullet)^{\mathrm{T}}$. With this transformation, $\vec{j}$ is trivially invariant, whereas $\vec{r}_4$ changes its sign. Therefore, the parity-odd quantity such as $\vec{r}_4\cdot\vec{j}$ vanishes.)

Together with the -perturbation by $\hat{T}_3$,

$$\langle 5^{(0)}|\hat{T}_3|5^{(0)}\rangle=-\left(\nu+\frac{1}{2}(\xi_1+\xi_2)\right)w_0+\frac{1}{4}\vec{r}_5\cdot(-\vec{k}+\vec{\ell}+\vec{m}), \tag{S.10}$$

with $\vec{k}$, $\vec{\ell}$ and $\vec{m}$ being the sum of the columns in K, L and M respectively, we obtain

$$\lambda_5=1+\left(-\frac{11}{2}w_0+\frac{1}{4}\vec{r}_5\cdot\vec{j}\right)g^2+\left\{-24w_0+\frac{1}{4}\vec{r}_5\cdot(-\vec{k}-\vec{\ell}+\vec{m})\right\}g^3+\mathcal{O}(g^4). \tag{S.11}$$

The degeneracy between λ_1 and λ_4 even under the influence of $\hat{T}_2$ is **removed** by $\hat{T}_3$ represented as

$$\langle l^{(0)}|\hat{T}_3|l'^{(0)}\rangle_{(l,l')\in\{1,4\}^2}=\begin{pmatrix}\frac{1}{4}\vec{1}\cdot(\vec{k}+\vec{\ell})-\nu w_0&\frac{1}{4}\vec{r}_4\cdot(\vec{k}+\vec{\ell})\\\frac{1}{4}\vec{1}\cdot(\vec{k}-\vec{\ell})&\frac{1}{4}\vec{r}_4\cdot(\vec{k}-\vec{\ell})-\nu w_0\end{pmatrix}=\begin{pmatrix}0&0\\0&\frac{1}{4}\vec{r}_4\cdot(\vec{k}-\vec{\ell})-\nu w_0\end{pmatrix}. \tag{S.12}$$

This leads to

$$\lambda_1=1,\qquad\lambda_4=1-\left\{5w_0-\frac{1}{4}\vec{r}_4\cdot\left(\vec{k}-\vec{\ell}\right)\right\}g^3+\mathcal{O}(g^4). \tag{S.13}$$

Perturbation in $\lambda^{(0)}_{2,3,8}=-1$ subspace

The $\lambda^{(0)}=-1$ eigenspace in the unperturbed system is spanned by the $l=2,3,8$ eigenvectors,

$$\langle l^{(0)}|\hat{T}_2|l'^{(0)}\rangle_{(l,l')\in\{2,3,8\}^2}=\begin{pmatrix}0&0&0\\0&0&0\\0&0&\frac{1}{2}(\mu_1+\mu_2)w_0+\frac{1}{4}\vec{r}_8\cdot\vec{j}_8\end{pmatrix}\quad\text{with}\quad\vec{j}_8\equiv J\begin{pmatrix}1\\-1\\1\\-1\end{pmatrix}. \tag{S.14}$$

Together with the perturbation by $\hat{T}_3$,

$$\langle 8^{(0)}|\hat{T}_3|8^{(0)}\rangle=\frac{\xi_1+\xi_2}{2}w_0+\frac{1}{4}\vec{r}_8\cdot\vec{m}_8,\quad\text{with}\quad\vec{m}_8\equiv M\begin{pmatrix}1\\-1\\1\\-1\end{pmatrix}, \tag{S.15}$$

$$\langle l^{(0)}|\hat{T}_3|l'^{(0)}\rangle_{(l,l')\in\{2,3\}^2}=\begin{pmatrix}\nu w_0+\frac{1}{2}\vec{r}_2\cdot\vec{k}_-&\frac{1}{2}\vec{r}_2\cdot\vec{\ell}_-\\\frac{1}{2}\vec{r}_3\cdot\vec{k}_-&\nu w_0+\frac{1}{2}\vec{r}_3\cdot\vec{\ell}_-\end{pmatrix}, \tag{S.16}$$

we have

$$\lambda_8=-1+\left(\frac{11}{2}w_0+\frac{1}{4}\vec{r}_8\cdot\vec{j}_8\right)g^2+\left(19w_0+\frac{1}{4}\vec{r}_8\cdot\vec{m}_8\right)g^3+\mathcal{O}(g^4), \tag{S.17}$$

and

$$\lambda_{2,3}=-1+\left\{\nu w_0+\frac{1}{4}(\vec{r}_2\cdot\vec{k}_-+\vec{r}_3\cdot\vec{\ell}_-)\pm\frac{1}{4}\sqrt{(\vec{r}_2\cdot\vec{k}_--\vec{r}_3\cdot\vec{\ell}_-)^2+4(\vec{r}_2\cdot\vec{\ell}_-)(\vec{r}_3\cdot\vec{k}_-)}\right\}g^3+\mathcal{O}(g^4). \tag{S.18}$$

Perturbation for $\lambda_{6,7}^{(0)} = \pm i$

The $\mathcal{O}(g^2)$ and $\mathcal{O}(g^3)$ perturbations on λ_6 are obtained from

$$\langle 6^{(0)}|\hat{T}_2|6^{(0)}\rangle = -\frac{1}{2}(\mu_1+\mu_2)w_0 i + \frac{1}{4}\vec{r}_6\cdot\vec{j}_6, \qquad \langle 6^{(0)}|\hat{T}_3|6^{(0)}\rangle = -\frac{1}{2}(\xi_1+\xi_2)w_0 i + \frac{1}{4}\vec{r}_6\cdot\vec{m}_6, \tag{S.19a}$$

where

$$\vec{m}_6 \equiv M\begin{pmatrix}1\\-i\\-1\\i\end{pmatrix}, \qquad \vec{j}_6 \equiv J\begin{pmatrix}1\\-i\\-1\\i\end{pmatrix}. \tag{S.19b}$$

One then finds

$$\lambda_6 = i + \Big(-\frac{11}{2}w_0 i + \frac{1}{4}\vec{r}_6\cdot\vec{j}_6\Big)g^2 + \Big(-19w_0 i + \frac{1}{4}\vec{r}_6\cdot\vec{m}_6\Big)g^3 + \mathcal{O}(g^4) \qquad \lambda_7 = (\lambda_6)^*. \tag{S.20}$$

These eigenvalues (S.11), (S.13), (S.17), (S.18) and (S.20) reveal the behaviors of this Markovian lattice model at low temperature. First, the stationary distribution after a long sequence generated by Eq.(2) is given by the $\lambda = 1$ eigenstate, $|1\rangle$. At the leading order, it is solely composed of the radial stripes, which directly shows the dynamical pattern selection. The $\mathcal{O}(g^2)$-perturbation (S.11) implies that the circular stripes decay to the radial stripes rather quickly with a lifetime of $\mathcal{O}(g^{-2})$. The shifts of the radial stripes (from ABAB… to CDCD… or BABA…, for example), corresponding to the decay of the modes of $|2\rangle$, $|3\rangle$ **or** $|4\rangle$, are much slower than that, with a lifetime of $\mathcal{O}(g^{-3})$.

Perturbation for eigenvectors

As well as the eigenvalues discussed above, the corresponding eigenvectors also receive perturbation,

$$\begin{aligned}|l\rangle &= |l^{(0)}\rangle + g^2|l^{(2)}\rangle + g^3|l^{(3)}\rangle + \mathcal{O}(g^4),\\ |l^{(2)}\rangle &= \sum_{\lambda_m^{(0)}\neq\lambda_l^{(0)}} \frac{\langle m^{(0)}|\hat{T}_2|l^{(0)}\rangle}{\lambda_l^{(0)}-\lambda_m^{(0)}}\,|m^{(0)}\rangle, \qquad |l^{(3)}\rangle = \sum_{\lambda_m^{(0)}\neq\lambda_l^{(0)}} \frac{\langle m^{(0)}|\hat{T}_3|l^{(0)}\rangle}{\lambda_l^{(0)}-\lambda_m^{(0)}}\,|m^{(0)}\rangle.\end{aligned} \tag{S.21}$$

In particular, for $l = 1,2,3,4$, we have $\hat{T}_2|l^{(0)}\rangle = 0$ leading to $|l^{(2)}\rangle = 0$. Because the similarity measures $I_R^{(l)}$ depend linearly on the state vectors, we obtain

$$I_*^{(l)} = \begin{cases}1+\mathcal{O}(g^3) & (l=1)\\ \mathcal{O}(g^3) & (l=2,3,4)\\ -1+\mathcal{O}(g^2) & (l=5)\\ \mathcal{O}(g^2) & (l=6,7,8)\end{cases}, \qquad I_\odot^{(l)} = \begin{cases}\mathcal{O}(g^3) & (l=1,2,3,4)\\ 1+\mathcal{O}(g^2) & (l=5)\\ \mathcal{O}(g^2) & (l=6,7,8)\end{cases}. \tag{S.22}$$

II. Numerical values of perturbative coefficients

Analytic formulas for $w = 8$

For $w = 4w_0 = 8$, we can explicitly compute the matrices P, Q, J, K, L, M and the resulting perturbative coefficients. The formula (S.7) for the "unperturbed" eigenvectors (including the effects up to $\hat{T}_{3/2}$) is expanded as

$$\vec{r}_l = \vec{x}_l\frac{P}{\lambda_l^{(0)}}\sum_{n=0}^{\infty}\left(\frac{Q}{\lambda_l^{(0)}}\right)^n, \tag{S.23}$$

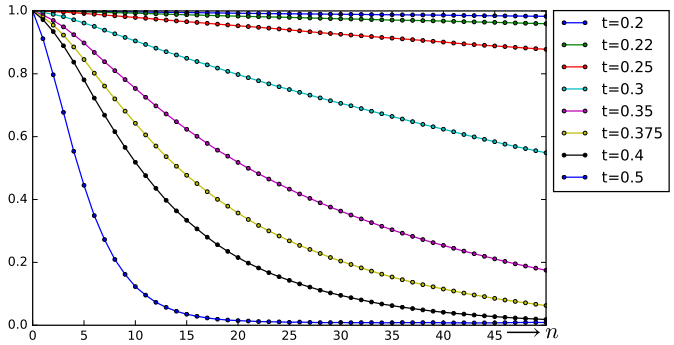

FIG. S.1: Plot of $I_\odot(n)$ by simulations for $w = 8$, averaged over 4096×4 trajectories under (E, F, G, H) initial configurations with equal weight for each temperature.

from which we can calculate the coefficients of $\vec{r}_l$ expanded in terms of g with a pretty good convergence by taking sum up to $n = 128$. Substituting them into (S.11), (S.13), (S.17), (S.18) and (S.20), we finally obtain the perturbative coefficients for λ_l as

$$\lambda_1 = 1, \tag{S.24a}$$
$$\lambda_{2,3} = -1 + \mathcal{O}(g^4), \tag{S.24b}$$
$$\lambda_4 = 1 - 10g^3 + \mathcal{O}(g^4), \tag{S.24c}$$
$$\lambda_5 = 1 - 5.8g^2 - 16.84g^{5/2} + 9.068g^3 - 371.5176\dot{7}40\dot{0}g^{7/2} + \mathcal{O}(g^4), \tag{S.24d}$$
$$\lambda_{6,7} = \pm\Big(1 - 5.8g^2 - 16.84g^{5/2} + 9.068g^3 + 324.1043\dot{4}0\dot{7}g^{7/2}\Big)i - 47.41\dot{3}g^{7/2} + \mathcal{O}(g^4), \tag{S.24e}$$
$$\lambda_8 = -1 + 5.8g^2 + 16.84g^{5/2} - 9.068g^3 + 276.6910\dot{0}7\dot{4}g^{7/2} + \mathcal{O}(g^4), \tag{S.24f}$$

where the dots represent recurring decimals. The true coefficients are known to be rational numbers, so that the above coefficients must be exact although obtained numerically. We find that $|\lambda_{5,6,7,8}|$ are degenerated up to $\mathcal{O}(g^3)$, and the $\mathcal{O}(g^{7/2})$ contributions start to break the degeneracy. Also, $\lambda_{6,7}$ acquire nonzero real parts from $\mathcal{O}(g^{7/2})$. We note that $\lambda_{2,3}$ are not perturbed from -1 up to $\mathcal{O}(g^{7/2})$: Their absolute values should eventually become smaller than 1 in higher orders due to the Perron-Frobenius theorem.

Numerical results for $w = 8$

The analytic result (S.24d) can be checked from the numerical result of $I_\odot(n)$ as a function of n. Shown in FIG. S.1 are the results of simulations for 4096×4 trajectories with equal-weight (E, F, G, H) initial configurations. Corresponding initial state at $n = 0$ is written as

$$\sum_l c_l |l\rangle = |1^{(0)}\rangle + |5^{(0)}\rangle, \tag{S.25}$$

which leads to the coefficient $\{c_l\}$ as

$$c_1 = 1, \qquad c_4 = \mathcal{O}(g^4), \qquad c_5 = 1 + \mathcal{O}(g^4), \qquad c_l = -\frac{\langle l^{(0)}|\hat{T}_2|5^{(0)}\rangle}{1 - \lambda_l^{(0)}} g^2 + \mathcal{O}(g^3) \quad (l \neq 1, 4, 5). \tag{S.26}$$

From (7) together with (S.22) and (S.26), we have

$$I_\odot(n) \simeq \lambda_5^n I_\odot^{(5)}, \tag{S.27}$$

in a range of n satisfying $1 \ll n \ll -g^{-2} \log g$. Therefore, we obtain

$$\lambda_5^{\text{eff}} \simeq \frac{I_\odot(n+1)}{I_\odot(n)}. \tag{S.28}$$

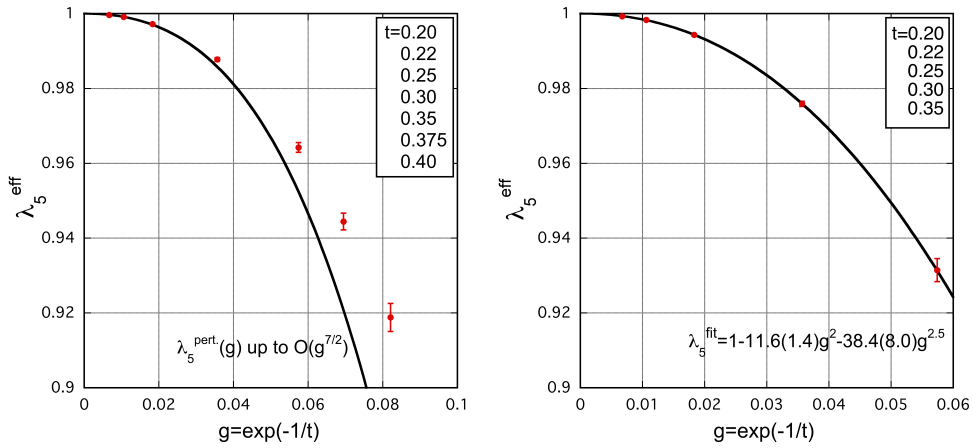

FIG. S.2: Ranges of $I_\odot(n+1)/I_\odot(n)$ for $10 \le n \le 30$ (red marks) and the perturbative λ_5 up to $g^{7/2}$-order (S.24d) (black curve), for $w = 8$ from the data of FIG. S.1 (left) and for $w = 16$ from that of FIG. 5 (right).

Plotted in the left panel of FIG. S.2 is a comparison of the analytic result of λ_5 in (S.24d) and the numerical result of $\lambda_5^{\rm eff}$ in (S.28). They show good agreement at low temperature ($t \le 0.25$), while the the discrepancy appears for $t \ge 0.3$ indicating the breakdown of the perturbative estimate at high temperature. By fitting the numerical data at $t = 0.2, 0.22, 0.25$ with an ansatz, $\lambda_5 = 1 - \gamma g^2 - \delta g^{5/2}$, we obtain

$$\gamma \simeq 5.78 \pm 1.82, \qquad \delta \simeq 20.2 \pm 10.5, \tag{S.29}$$

which are quite consistent with analytic results in (S.24d); $(\gamma, \delta) = (5.8, 16.84)$.

Numerical results for $w = 16$

For $w = 4w_0 = 16$, it is numerically demanding to obtain the analytic formula similar to (S.24). Nevertheless, we can extract the coefficients γ and δ by plotting $\lambda_5^{\rm eff}$ in (S.28) as shown in the right panel of FIG. S.2. By fitting the data at $t = 0.2, 0.22, 0.25, 0.30, 0.35$, we find

$$\gamma \simeq 11.6 \pm 1.4, \qquad \delta \simeq 38.4 \pm 8.0. \tag{S.30}$$

These results together with (S.27) lead to the temperature dependence of the decay rate of the circular stripe pattern as given in the main text.

III. Mechanism of DPS in a Minimal Model

To identify the essential origin of the dynamical pattern selection (DPS), let us consider a minimal toy-model with only 3 states (rather than 6^w states discussed in the main text). They represent two stable patterns (which we call X and Y) and a transition state (Z). They have intra energies $B^{(\rm intra)}_{X,Y,Z}$ and and the inter binding energies $B^{(\rm inter)}_{YX,ZX,ZY}$ and obey the Markov chain with Eq.(3). The transition matrix at zero temperature ($t = 0$) is given as

$$\hat{T}_0 = \begin{array}{c} \begin{matrix} X & Y & Z \end{matrix} \\ \begin{pmatrix} 1 & 0 & p_1 \\ 0 & 1 & p_2 \\ 0 & 0 & q \end{pmatrix} \end{array}, \tag{S.31}$$

where $p_{1,2}$ and q are positive with the constraint $p_1+p_2+q=1$. The eigenvalues of this matrix is $\lambda^{(0)}=1,q$, and we define the corresponding basis vectors as

$$\langle 1|=\left(1,0,\frac{p_1}{p_1+p_2}\right),\quad |1\rangle=\begin{pmatrix}1\\0\\0\end{pmatrix};\quad \langle 2|=\left(0,1,\frac{p_2}{p_1+p_2}\right),\quad |2\rangle=\begin{pmatrix}0\\1\\0\end{pmatrix};\quad \langle 3|=(0,0,1),\quad |3\rangle=\begin{pmatrix}-\frac{p_1}{1-q}\\-\frac{p_2}{1-q}\\1\end{pmatrix}. \tag{S.32}$$

For small nonzero temperature, $0<t\ll 1$, we perturb the transition matrix as $\hat{T}=\hat{T}_0+\delta\hat{T}$ by

$$\delta\hat{T}=\begin{pmatrix}-a-a' & b' & c\\ a' & -b-b' & d\\ a & b & e\end{pmatrix}, \tag{S.33}$$

where $a,b,a',b'>0$. In terms of the binding energies,

$$\begin{aligned}
a&=\frac{p_X e^{-\beta\mathcal{E}_{ZX}}}{p_X e^{-\beta\mathcal{E}_{XX}}+p_Y e^{-\beta\mathcal{E}_{YX}}+p_Z e^{-\beta\mathcal{E}_{ZX}}}\sim e^{-\beta(\mathcal{E}_{ZX}-\mathcal{E}_{XX})},\\
b&=\frac{p_X e^{-\beta\mathcal{E}_{ZY}}}{p_X e^{-\beta\mathcal{E}_{XY}}+p_Y e^{-\beta\mathcal{E}_{YY}}+p_Z e^{-\beta\mathcal{E}_{ZY}}}\sim e^{-\beta(\mathcal{E}_{ZY}-\mathcal{E}_{YY})},\\
a'&=\frac{p_X e^{-\beta\mathcal{E}_{YX}}}{p_X e^{-\beta\mathcal{E}_{XX}}+p_Y e^{-\beta\mathcal{E}_{YX}}+p_Z e^{-\beta\mathcal{E}_{ZX}}}\sim e^{-\beta(\mathcal{E}_{YX}-\mathcal{E}_{XX})},\\
b'&=\frac{p_X e^{-\beta\mathcal{E}_{ZY}}}{p_X e^{-\beta\mathcal{E}_{XY}}+p_Y e^{-\beta\mathcal{E}_{YY}}+p_Z e^{-\beta\mathcal{E}_{ZY}}}\sim e^{-\beta(\mathcal{E}_{ZY}-\mathcal{E}_{YY})}.
\end{aligned} \tag{S.34}$$

where $\mathcal{E}_{ij}$'s are defined in the same way as Eq.(3).

Projected on the $\lambda^{(0)}=1$ unperturbed eigenspace, $\delta\hat{T}$ becomes

$$\langle l^{(0)}|\delta\hat{T}|l'^{(0)}\rangle_{(l,l')\in\{1,2\}^2}=\begin{pmatrix}-\frac{p_2}{p_1+p_2}a-a' & \frac{p_1}{p_1+p_2}b+b'\\ \frac{p_2}{p_1+p_2}a+a' & -\frac{p_1}{p_1+p_2}b-b'\end{pmatrix}, \tag{S.35}$$

whose eigenvalues read

$$\delta\lambda_1=0,\quad \delta\lambda_2=-(a+b+a'+b'). \tag{S.36}$$

Corresponding eigenvectors in the original 3-dimensional space are

$$|1\rangle=\begin{pmatrix}p_1b+(p_1+p_2)b'\\ p_2a+(p_1+p_2)a'\\ 0\end{pmatrix},\qquad |2\rangle=\begin{pmatrix}-1\\1\\0\end{pmatrix}. \tag{S.37}$$

Then in the first-order perturbation theory, $|1\rangle$ is the eigenvector of $\hat{T}$ for the eigenvalue $\lambda=1$, i.e., it represents the stationary distribution of the system.

When p_1 and p_2 are of the same order, which one of X and Y dominates the steady distribution is determined by which of $\max\{a,a'\}$ and $\max\{b,b'\}$ is larger than the other. From (S.34), the magnitude of $\max\{a,a'\}$ ($\max\{b,b'\}$) corresponds to the minimum excitation energy from X (Y). If we define

$$\Delta\mathcal{E}_X=\min\{\mathcal{E}_{ZX},\mathcal{E}_{YX}\}-\mathcal{E}_{XX},\quad \Delta\mathcal{E}_Y=\min\{\mathcal{E}_{ZY},\mathcal{E}_{XY}\}-\mathcal{E}_{YY}, \tag{S.38}$$

then $\Delta\mathcal{E}_X>\Delta\mathcal{E}_Y$ ($\Delta\mathcal{E}_X<\Delta\mathcal{E}_Y$) indicates that $|1\rangle\simeq(1,0,0)^{\mathrm{T}}$ ($|1\rangle\simeq(0,1,0)^{\mathrm{T}}$), i.e. the pattern X (Y) is dynamically selected. Also, the mean-number of steps $\bar{n}$ for the unstable pattern to decay is derived from (S.36) as

$$\bar{n}^{-1}=-\ln\lambda_2\sim e^{-\beta\min\{\Delta\mathcal{E}_X,\Delta\mathcal{E}_Y\}}. \tag{S.39}$$

Although we analyzed the minimal 3-state model here, it is straightforward to generalize it to a full-scale model with a block structure,

$$\hat{T}_0 = \begin{pmatrix} S_1 & 0 & P_1 \\ 0 & S_2 & P_2 \\ 0 & 0 & Q \end{pmatrix}, \tag{S.40}$$

which includes the case of the 6^w-state model discussed in the main text and in (S.2). In this context, X (Y) in the minimal model corresponds to the radial stripes $\{A, B, C, D\}$ (circular stripes $\{E, F, G, H\}$). Also $|1\rangle$ ($|2\rangle$) in the minimal model corresponds to $|1\rangle$ in Eq.(S.6e) ($|5\rangle$ in Eq.(S.6e)). Then, the stability of the radial stripes is a result of

$$\Delta\mathcal{E}_* = \sigma > \sigma' = \Delta\mathcal{E}_\odot. \tag{S.41}$$